Bound states in photonic Fabry-Perot resonator with nonlinear off-channel defects

Evgeny N. Bulgakov[1,2] and Almas F. Sadreev[1]
[1]*Institute of Physics, Academy of Sciences, 660036 Krasnoyarsk, Russia*
[2]*Siberian State Aerospace University, Krasnoyarsk Rabochii, 31, Krasnoyarsk, Russia*
(Received 4 December 2009; revised manuscript received 28 January 2010; published 18 March 2010)

We consider a Fabry-Perot resonator (FPR) comprised of two off-channel nonlinear defects coupled to the photonic waveguide. For the linear case FPR can support bound states in the form of standing waves between the defects if a distance between them is quantized. For the nonlinear case the bound states appear for arbitrary distance between the defects if electromagnetic intensity is quantized. For transmission through the FPR we reveal additional resonances which are the result of coupling of incident wave with the bound states because of nonlinearity of the defects. The resonances are spaced at the eigenfrequencies of bound states with a width proportional to the input amplitude. The theory of the FPR based on the simple Wang and Fan model [Phys. Rev. E **68**, 066616 (2003)] is complemented by the tight-binding one. The results for the transmission and bound states in these models agree with computations in real two-dimensional photonic crystal waveguide coupled with two off-channel defects fabricated from a Kerr-type material.

DOI: 10.1103/PhysRevB.81.115128 PACS number(s): 42.70.Qs, 05.60.Gg, 41.20.Jb, 42.79.Gn

I. INTRODUCTION

It is believed that future integrated photonic circuits for ultrafast all-optical signal processing require different types of nonlinear functional elements such as switches, memory, and logic devices. Therefore, both physics and designs of such all-optical devices have attracted significant research efforts during the last two decades and most of these studies utilize the concepts of optical switching and bistability. One of the simplest bistable optical devices which can be built up in photonic integrated circuits is a single planar nanocavity coupled with optical waveguide or waveguides.[1] Its transmission properties depend on the intensity of incident light when the cavity is made of a Kerr nonlinear material. If the characteristic optical wavelength much exceeds the size of the nonlinear cavity, it can be presented by single isolated nonlinear mode coupled with the waveguide. Thereby the system becomes equivalent to the single level nonlinear Fano-Anderson model that describes nonlinear impurity embedded in a continuum. The system attracts interest over decade because of analytical treatment and its generality.[2–12] On the other hand, the system can be realized in the two-dimensional photonic crystals (PhC).

The one-dimensional layered PhC with, at least, one thick layer made of the Kerr material is the another example that admits analytical solution by means of the one-dimensional nonlinear Schrödinger equation.[13–15] As different from the former case of nonlinear impurity the last case presents extended nonlinear object but both cases demonstrate bistability effects in the transmission. However the single nonlinear impurity built up into the linear chain (the in-channel defect) is remarkable by that the eigenfrequency below the propagation band of the chain might appear with growth of the nonlinearity constant. Then the corresponding eigenfunction becomes localized, i.e., the in-channel nonlinear defect can give rise to the bound state.[2,3,9]

One may ask does exist the localized bound state with discrete eigenfrequency inside the propagation band. First, this question was formulated and positively answered by von Neumann and Wigner in 1929.[16] Their analysis examined by Stillinger and Herrick[17] was long time regarded as mathematical curiosity because of certain spatially oscillating central symmetric potentials. However in 1973 Herrik[18] and Stillinger[19] predicted BSCs in semiconductor heterostructure superlattices observed by Capasso *et al.*[20] as a very narrow absorption peak. In the last time the phenomenon of BSC attracted large interest in application to different systems,[21] in particular, in highly promising photonic crystals.[22–26] The BSC has no coupling with continuum (waveguide) and, therefore, cannot be excited by transmitted wave[27,28] in linear systems. It can be traced by narrowing of the resonance width for approaching to the BSC point for a variation in physical parameters of the system.[20,29,30] In particular, in open quantum dots the BSC point could be achieved by a variation in the confined potential, i.e., by the variation in gate potential.[27] In PhC the BSC appears for tuning of dielectric constant of the defects.[23] Therefore in linear systems this phenomenon is rather subtle one.

Recently it was shown in framework of the two-level nonlinear Fano-Anderson model that a BSC scenario described in Refs. 27 and 29–31 develops by a self-induced way because of the nonlinearity.[32] Moreover, an incident wave interacts with the BSC that gives rise to a resonance of peculiar shape at the vicinity of the BSC eigenfrequency. The PhCs with, at least, two defects of a Kerr media are the best candidates for realization of these phenomena. In present paper we consider the PhC structure with two nonlinear defects that forms the Fabry-Perot resonator (FPR).

The typical FPR consists of two plane mirrors at the distance L and dielectric media with the refractive index n between. Then the transmission through the FPR can be easily found as geometric sum of consequent transmissions and reflections through each mirror specified by t_1 and r_1,[15,33]

$$t = \frac{t_1^2 \exp(ikL)}{1 - r_1^2 \exp(2ikL)}, \tag{1}$$

where $k = \omega n/c$ is the wave number in a media. Assume the mirrors are perfect ($r_1 = 1$). Then the BSC that does not leaks

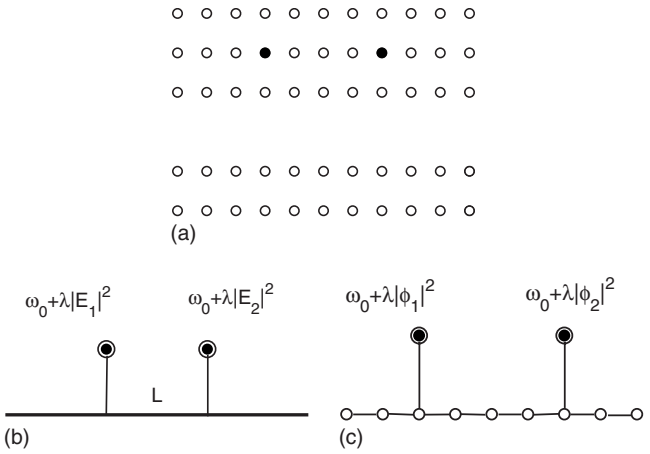

FIG. 1. (a) Photonic crystal consists of a square lattice of dielectric rods. A single row of rods is extracted to form one-dimensional directed waveguide. Two nonlinear defect rods marked by filled circles are inserted into the photonic crystal. (b) The nonlinear model of FPR. (c) The tight-binding version of the photonic crystal system in (a), respectively.

through the mirrors arises at $kL=\pi m$, where m are integers. Therefore, the underlying mechanism of the bound states in the FPR is (i) perfect reflections at mirrors and (ii) the integer number of the half waves is to be spaced between mirrors. The BSCs are accomplished by crossing of the zero transmission with the unit one[27] and displays in frequency dependence of the transmission as a collapse of the Fano resonance[34] [see Fig. 7(a)]. This mechanism for the BSCs, exclusively transparent, was applied to photonic crystal structure with one and two waveguides coupled with two single-mode cavities,[23,35–38] to typical one-dimensional double-barrier structure with temporally periodically driven potential of barrier[39] and two identical quantum dots connected by wire.[40–42]

We consider here the single-channel waveguide in a PhC coupled with two off-channel single-mode nonlinear cavities (defects) which can be interpreted as nonlinear mirrors. The reader is reminded that PhC is a periodic array of dielectric medium[1] having electromagnetic modes that are Bloch waves with a frequency spectrum separated into a series of pass and stop bands. We consider a square array of parallel, infinitely long high dielectric rods in air. The removal of a row of rods breaks the periodicity in one spatial direction. If the parameters of the crystal are such that there is a complete band gap for wave vectors perpendicular to the rods, then this defect can introduce modes that decay exponentially away from the defect but can still be described by a wave vector pointing along the missing row of rods. Such a row a defects acts like a waveguide.[1] Next, following, for example, Refs. 38, 43, and 44 we introduce two planar-PhC nanocavities (defects) coupled with the photonic waveguide as shown in Fig. 1(a). The cavity supports a localized nondegenerate monopole solution for the TM modes that has the electric field component parallel to the cylinders.[45,46] The two cavity modes might be evanescently coupled to each other. However in what follows we neglect by this direct interaction of the cavities. They are also coupled to the PhC waveguide. Each off-channel defect gives rise to the interference of electromagnetic waves flowing over the waveguide and through the off-channel defect, i.e., to the Fano resonance. It results in zero transmission at the defect's eigenfrequency ω_0 for the linear case provided that this frequency belongs to propagation band of the waveguide.[1] Therefore the off-channel defects may serve as perfect mirrors however only at the frequency $\omega=\omega_0$ at which $r_1(\omega_0)=1$. Then the BSC with the eigenfrequency $\omega_c=\omega_0$ might appear between the off-channel defects if the equation

$$\theta_m = k(\omega_0)L = \pi m \tag{2}$$

is fulfilled. The dispersion $k(\omega)$ is defined by a specific PhC. It can be done provided that the distance L between defects is quantized that is hard to achieve in the discrete PhC lattice. Another way is to tune the eigenfrequency of the defects ω_0. Thus, for the linear PhC systems the phenomenon of formation of the BSC is rather subtle one.

We take the medium of the defects is nonlinear via the third-order Kerr nonlinearity, i.e., the refractive index of the defects changes instantaneously with the optical intensity. The system of one nonlinear impurity embedded in a one-dimensional continuum attracted interest long time ago because of analytical treatment and its generality.[2,5–7,9] The system is open and differs from closed nonlinear counterpart by that the transmission resonance properties depend on the amplitude of incident wave. Correspondingly we can govern the resonance by the field intensity at the defects to give rise to a bistability. Similar effects were shown for the finite cluster of two nonlinear off-channel sites coupled to the linear waveguide.[11,12,25,47–49]

The dielectric constant of defect rods formed from a Kerr medium depends on the electric field at the defects[50,51]

$$\epsilon_d(\mathbf{r}) = \epsilon_0 + \mathrm{Re}[\chi^{(3)}]|E(\mathbf{r})|^2. \tag{3}$$

The frequency of isolated bound mode for the single defect rod decreases monotonously with growth of its dielectric constant ϵ_d.[23,46] Therefore the mode frequencies of the defects enumerated by $j=1,2$ for the radius much less than the electromagnetic (EM) wavelength undergo shifts

$$\omega_j = \omega_0 + \lambda|E_j|^2. \tag{4}$$

The transmission through each off-channel defect has zero (resonance dip) at these eigenfrequencies.[7] In order to have perfect mirrors, the transmission zeros of both defects should occur at the same frequency

$$\omega_c = \omega_0 + \lambda X_c = \omega_0 + \lambda Y_c, \tag{5}$$

where $X=|E_1|^2$ and $Y=|E_2|^2$ are intensities of electromagnetic wave at the first and second defects, respectively. This equation establishes equaled intensities at the defects: $X_c=Y_c$. The boundary condition for the BSC between nonlinear mirrors gives us the following equation for the intensity X_c:

$$k(\omega_c)L = k(\omega_0 + \lambda X_c)L = \pi m, \quad m = 0,1,2,\ldots, \tag{6}$$

where k is the wave number of the electromagnetic wave propagated along the waveguide that is the function of the frequency ω. For the linear case $\lambda=0$ this equation can be satisfied by a quantization of the distance between the mir-

rors only or by tuning of the defect's eigenfrequency ω_0 as was discussed above. However for the nonlinear case Eq. (6) can be fulfilled by a shift of the defect eigenfrequency [Eq. (4)]. In other words, the FPR supports BSCs for arbitrary distance between mirrors provided however that the intensity of light X_c is quantized at the defects. For the transmission through the two-level nonlinear Fano-Anderson model we revealed additional resonances because of coupling of incident wave with BSC via nonlinearity.[32] Respectively, we expect similar resonances at the eigenfrequencies of the BSCs in the FPR with nonlinear mirrors. In order to consider these effects in detail we explore, first, the most simple coupled-mode theory.[22,35–38] Also we use the tight-binding version of this theory that is more close to the real PhC structures. We complement these model results by computer simulations of real PhC structures shown in Fig. 1(a) and show full qualitative agreement of the numerical results with theory.

II. BASIC EQUATIONS

The transmission of TM modes in linear PhC structures is equivalent to quantum transmission.[1] Thereby basic equations for the transmission in the PhC structures can be derived from the Lippman-Schwinger (LS) equation as was done in Refs. 23, 36, and 43, from the coupled-mode theory,[22,37,52] or one can explore the tight-binding models with further continual limit $ka \ll 1$. In the present paper we show that all approaches give qualitatively the same results for the case of nonlinear defects. We start with the temporal couple-mode theory and apply it for the case the waveguide coupled with the single nonlinear off-channel defect. That case was considered in many works[5–7,53] to show a bistability of the transmission. Let a monochromatic wave $E_{in}e^{-i\omega t}$ incidents at the left. Then we can write for the defect amplitudes

$$\dot{E} = -i\omega_1 E - \frac{2}{\tau}E + \sqrt{\frac{2}{\tau}}E_{in}e^{-i\omega t}, \tag{7}$$

where $\omega_1 = \omega_0 + \lambda|E_1|^2$ is the frequency of the defect oscillations which undergoes a shift in accordance to Eq. (4). This equation has simple physical meaning. Because of coupling of the defect mode with the continuum of waveguide the mode leaks with the decay time τ. Simultaneously owing to the same coupling constant $\sqrt{\Gamma} = \sqrt{\frac{2}{\tau}}$ the source in the form of incident wave in the right hand of Eq. (7) supports the defect mode. Next, we can substitute the time dependence as $E(t) = Ee^{-i\omega t}$ and present Eq. (7) as follows:

$$(\omega - \omega_1 + i\Gamma)E = i\sqrt{\Gamma}E_{in}. \tag{8}$$

Further we can write for the transmission amplitude with account of interference of direct path over the waveguide and the path through the off-channel defect. Following[33,52] we write $|out\rangle = S|inc\rangle + E|V\rangle$ where the outgoing waves are collected in the column $|out\rangle = \begin{pmatrix} r \\ t \end{pmatrix}$, the incoming waves are collected in the column $|inc\rangle = \begin{pmatrix} E_{in} \\ 0 \end{pmatrix}$, S is the S-matrix which for our case of the single waveguide has the form $S = \begin{pmatrix} 0 & 1 \\ 1 & 0 \end{pmatrix}$, and the column $|V\rangle = \begin{pmatrix} g \\ g \end{pmatrix}$ consists of the coupling constant g, and t and r are the transmission and reflection amplitudes. From the unitarity of the scattering processes $\langle out|out\rangle = |t|^2 + |r|^2 = E_{in}^2$ and use of the solution of Eq. (8) we obtain $g = -\sqrt{\Gamma}$.[52] Therefore, we obtain for the transmission and reflection amplitudes for this tutorial case of the single off-channel nonlinear defect

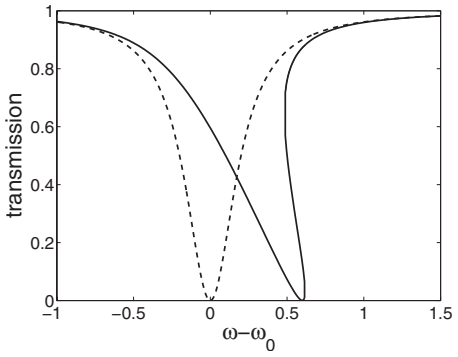

FIG. 2. Transmission spectra of the single off-channel nonlinear defect given by Eq. (9) for $\lambda = 0.2$ and $\Gamma = 1$. The dash line shows the linear case. The nonlinearity shifts the eigenfrequency of the defect at which the transmission equals zero.

$$t = E_{in} - \sqrt{\Gamma}E, \quad r = -\sqrt{\Gamma}E. \tag{9}$$

One can see that for $E = 0$ there is no reflection. Finally we are to write the equation of self-consistency for the intensity of light at the off-channel nonlinear defect

$$X[(\omega - \omega_0 - \lambda X)^2 + \Gamma^2] = \Gamma E_{in}^2. \tag{10}$$

This equation is equivalent to Eq. (13) of Ref. 7 with accuracy of notations. Correspondingly we have similar bistable behavior of the transmission $|t_1^2/E_{in}^2$ shown in Fig. 2. The perfect reflection takes place at $\omega = \omega_0 + \lambda X$.[1,7]

Now we can easily write the coupled-mode theory equations for the case of two identical defects separated by distance L with corresponding amplitudes E_1 and E_2 (see, for example, Ref. 37),

$$(\omega - \omega_1 + i\Gamma)E_1 + i\Gamma e^{i\theta}E_2 = i\sqrt{\Gamma}E_{in},$$

$$i\Gamma e^{i\theta}E_1 + (\omega - \omega_2 + i\Gamma)E_2 = i\sqrt{\Gamma}e^{i\theta}E_{in}, \tag{11}$$

and the transmission amplitude

$$t = E_{in}e^{i\theta} - \sqrt{\Gamma}E_1 e^{i\theta} - \sqrt{\Gamma}E_2, \tag{12}$$

where $\theta = k(\omega)L$ represents the phase shift incurred as the waveguide mode travels from the first defect to the second one. The case of different defects will be considered below. From Eq. (11) we obtain

$$E_1 = \frac{i\sqrt{P}[\tilde{\omega} + \epsilon + i\Gamma(1 - e^{2i\theta})]}{\tilde{\omega}^2 - \epsilon^2 + 2i\Gamma\tilde{\omega} - \Gamma^2(1 - e^{2i\theta})},$$

$$E_2 = \frac{i\sqrt{P}e^{i\theta}(\tilde{\omega} - \epsilon)}{\tilde{\omega}^2 - \epsilon^2 + 2i\Gamma\tilde{\omega} - \Gamma^2(1 - e^{2i\theta})}, \tag{13}$$

where

$$\tilde{\omega} = \omega - \frac{\omega_1 + \omega_2}{2} = \omega - \omega_0 + \frac{\lambda}{2}(X+Y),$$

$$\epsilon = \frac{\omega_1 - \omega_2}{2} = \frac{\lambda}{2}(X-Y), \tag{14}$$

the value $P=\Gamma|E_{in}|^2$ is proportional to the input wave power. Substituting Eq. (13) into Eq. (14) we obtain the nonlinear self-consistent equations for EM intensities X and Y at each defect

$$X[(\tilde{\omega}^2 - \epsilon^2 - 2\Gamma^2 \sin^2\theta)^2 + \Gamma^2(2\tilde{\omega} + \Gamma \sin 2\theta)^2]$$
$$= P[(\tilde{\omega} + \epsilon + \Gamma \sin 2\theta)^2 + \Gamma^2 \sin^4\theta],$$

$$Y[(\tilde{\omega}^2 - \epsilon^2 - 2\Gamma^2 \sin^2\theta)^2 + \Gamma^2(2\tilde{\omega} - \sin 2\theta)^2] = P(\tilde{\omega} - \epsilon)^2. \tag{15}$$

The coupled mode [Eq. (11)] is the LS equation[36,54] and can be rewritten in the matrix form

$$(\omega - H_{eff})\begin{pmatrix} E_1 \\ E_2 \end{pmatrix} = i\sqrt{\Gamma}E_{in}\begin{pmatrix} 1 \\ e^{i\theta} \end{pmatrix}, \tag{16}$$

where the symmetric complex matrix H_{eff} ("the non-Hermitian effective Hamiltonian") can be easily found from Eqs. (11) and (16) to be equaled to

$$H_{eff} = \begin{pmatrix} \omega_1 - i\Gamma & -i\Gamma e^{i\theta} \\ -i\Gamma e^{i\theta} & \omega_2 - i\Gamma \end{pmatrix}. \tag{17}$$

The solution of the LS equation is given by the inverse of the matrix $(\omega - H_{eff})$. However there might be the case for the inverse does not exist, i.e., the determinant of the matrix equals zero. It is easy to see that it happens if the following equations are fulfilled

$$\tilde{\omega}^2 - \epsilon^2 - 2\Gamma^2 \sin^2\theta = 0, \quad \tilde{\omega} = -\Gamma \sin\theta \cos\theta$$

at points

$$\epsilon = 0, \quad \tilde{\omega} = 0, \quad \theta_m = \pi m, \tag{18}$$

where m is the integer. Then the solution of the homogeneous LS Eq. (16) takes the following form:

$$E_1 + (-1)^m E_2 = 0. \tag{19}$$

Therefore the BSC intensities at both defects are coincided: $X_c = Y_c$. The second equation in Eq. (18) defines the frequency of this special case given by Eq. (5): $\omega_c = \omega_a$ and $a = 1, 2$. At last, the third equation in Eq. (18) implies the quantization condition given by Eq. (6) that means that integer number of half wavelengths is placed between mirrors to form the BSC. In order the states were ideally trapped between the mirrors they are to have perfect reflection. In other words, the transmission probability through the each off-channel defect is to be equal to zero. As shown in Fig. 2 the off-channel defect perfectly reflects at the eigenfrequencies.

If the defects were linear we would have the quantization condition for the distance between defects $\theta = k(\omega_0)L = \pi m$. This well-known result about trapping of wave between mirrors[36,37] can be interpreted from more general position.[23]

If the determinant of the matrix $(\omega - H_{eff})$ equals zero, then the equation for eigenstates and eigenvalues for the non-Hermitian effective Hamiltonian

$$H_{eff}|bound\rangle = \omega|bound\rangle \tag{20}$$

has solution with the eigenvalue ω and with corresponding eigenstate $|bound\rangle = E_1\binom{1}{-e^{i\theta_m}} = E_1\binom{1}{-(-1)^m}$. In general, the complex eigenvalues of the effective Hamiltonian determine the positions and widths of the resonance states.[55–57] Therefore Eq. (20) defines the special case of the state with real eigenenergy. Comparison to Eq. (16) shows that Eq. (20) constitutes a homogeneous part of the LS Eq. (16), i.e., the solution $|bound\rangle$ exists regardless of the continuum. The state $|bound\rangle$ is orthogonal to the continuum state in the right-hand part of Eq. (16), i.e., has no coupling with the continuum. Because of that the state $|bound\rangle$ will not decay into the continuum and can be defined as the BSC. Such a solutions in application to the photonic crystal FPR are found in Refs. 22–24 and 26. For the photonic FPR with nonlinear defect rods the patterns of BSC are presented below.

The dispersion relations of the propagating guided modes $\omega(k)$ depend on specific PhC waveguide.[23,46] However in the vicinity of the defect eigenfrequency ω_0 we can use the approximation $k(\omega) \approx k(\omega_0) + k'(\omega_0)(\omega - \omega_0)$. Respectively, the phase shift in Eq. (11) can be written as

$$\theta \approx \theta_0 + \theta_1(\omega - \omega_0), \tag{21}$$

where $\theta_0 = k(\omega_0)L$ and $\theta_1 = k'(\omega_0)L$. Then the condition for the BSCs [Eq. (6)] can be easily solved to obtain

$$X_{cm} = \frac{\pi m - \theta_0}{\lambda \theta_1} \geq 0, \quad \omega_{cm} = \omega_0 + \frac{\pi m - \theta_0}{\theta_1}. \tag{22}$$

Thus, as different from the linear case the nonlinear off-channel defects can trap wave with quantized values of the intensity $X_{cm} = Y_{cm}$ at the defects irrespective to their eigenfrequency ω_0 and the distance between them. From relation between the amplitude of wave after the off-channel defect a, the amplitude at the defect E_1, and the amplitude of the incident wave E_{in}, we have $a = \sqrt{2\Gamma_1}E_1 + E_{in}$. Thus, for the BSCs the EM field intensity is quantized not only at the off-channel nonlinear defects but also between with the intensity $|a_m|^2 = 2\Gamma X_{cm}$.

The results of numerical calculation of the intensities X and Y for $E_{in} \neq 0$ that obey the self-consistent nonlinear [Eq. (15)] are shown in Fig. 3. Blow up in Fig. 3(b) demonstrates that these solutions have rather complicated form which shrink to the BSC points X_c and ω_c given by Eq. (22) if the input amplitude tends to zero as shown in Fig. 3(c). Numerical substitution of X and Y into Eqs. (14) and (12) consequently allows us to calculate the transmission spectra shown in Fig. 4. For specific numerical calculation we took $\lambda = 0.2$, $\omega_0 = 1$, $\theta_0 = 0.7\pi$, and $\theta_1 = \pi$. If to substitute these values into Eq. (22) we obtain that the BSC frequencies equal $0.3 + m = 0.3, 1.3, 2.3, \ldots$ and the intensities do $5(0.3+m) = 1.5, 6.5, 11.5, \ldots$. One can see that these discrete values of the frequency completely agree with positions of new resonances in Figs. 3 and 4 and discrete values of the intensity agree with set of branches for X and Y in Fig. 3 for $E_{in} \to 0$.

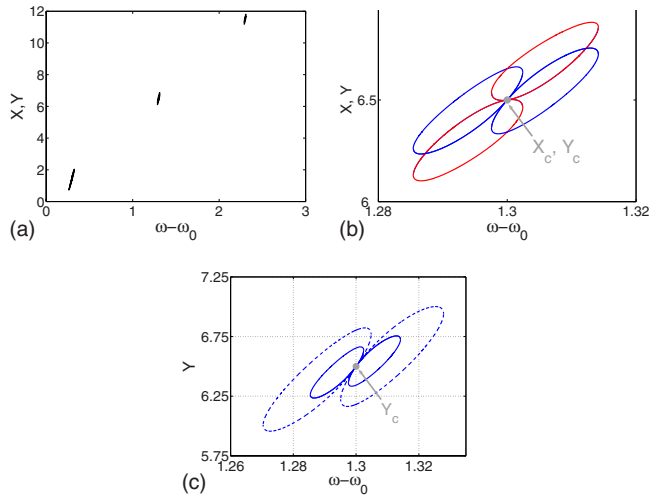

FIG. 3. (Color online) (a) Numerical solution of Eq. (15) for the parameters $\Gamma=1$, $\theta_0=0.7\pi$, $\theta_1=\pi$, $\lambda=0.2$, and $E_{in}=0.1$. (b) Blow up of the solution for X (red line) and Y (blue line) around the second BSC point $X_{c2}=Y_{c2}=6.5$ and $\omega_{c2}=1.3$. (c) Change in the intensity at the second defect under increasing of the input amplitude two times. Respectively, solid line shows Y at $E_{in}=0.1$ and dashed line shows Y at $E_{in}=0.2$.

As seen from Fig. 4(a) that there are two types of the transmission spectra. One type shown by dash line inherits from the linear FPR and coincides with its spectra for $E_{in}\to 0$.

A picket-fence type of resonances shown by solid line in Fig. 4(a) forms the second type of the transmission spectra. The origin of these resonances is considered in the nonlinear two-level Fano-Anderson model[32] and related to coupling of

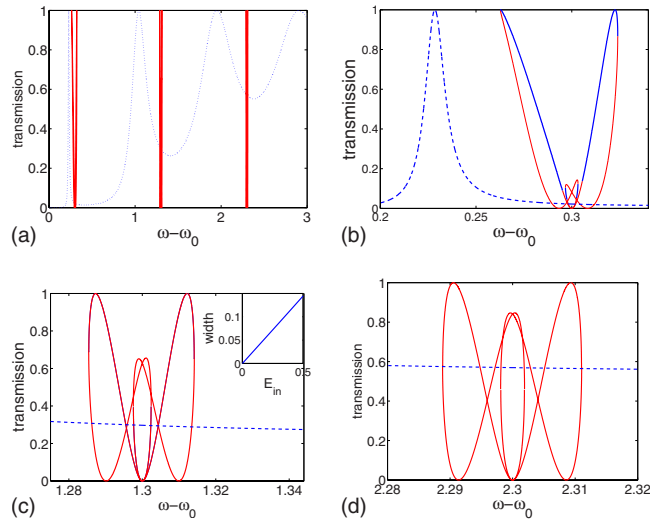

FIG. 4. (Color online) (a) Transmission spectra as dependent on frequency in the FPR given by Eq. (11) for the nonlinear case $\lambda=0.2$. The parameters of the FPR are given in Fig. 2. The dash line shows the transmission that slightly differs from the transmission in the linear FPR and solid line does a picket-fence resonances induced by BSCs (BSC induced resonances). Blows up of the BSC resonances for the BSC frequency equaled to (b) 0.3, (c) 1.3, and (d) 2.3, respectively. In Fig. 4(b) blue lines show unstable branches of the solution while red lines do the stable branches.

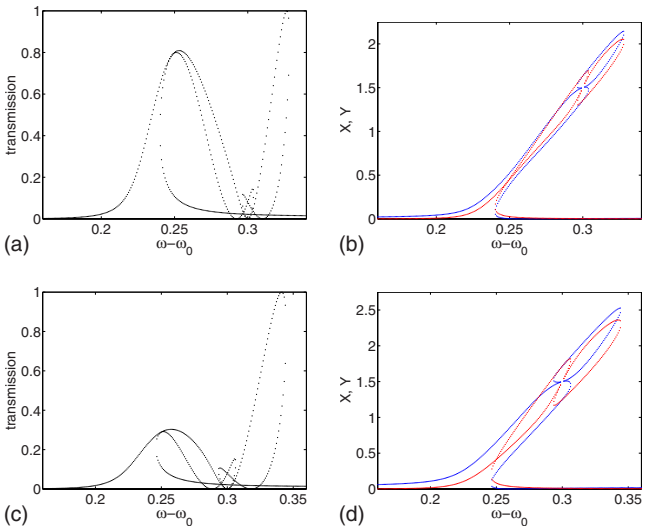

FIG. 5. (Color online) Transmission spectra and intensities at the off-channel defects as dependent on the frequency in FPR with growth of the incident amplitude [(a) and (c)] $E_{in}=0.12$ and [(b) and (d)] $E_{in}=0.2$. Other parameters of the FPR are given in Fig. 3.

the incident wave with the BSCs in FPR because of nonlinearity. A width of BSC induced resonance (for brevity BSC resonance) linearly grows with the amplitude of the incident wave E_{in} as inset in Fig. 4(c) shows. The width was determined by a frequency domain in which the new branch of the transmission exists. For example, for the branch shown in Fig. 4(c) the width approximately equals 0.027 for $E_{in}=0.1$. That result is similar to found in the nonlinear Fano-Anderson model.[32] However the nonlinear two-level Fano-Anderson model displays the only BSC resonance while the nonlinear FPR in the framework of the coupled-mode equations does picket fence like set of the BSC resonances that follows formula (22).

It is well known that some branches of the solution of nonlinear equation might be unstable. We performed stability analysis of the steady-state roots of Eq. (15), determined by linearizing the time-dependent coupled-mode equations.[1,22,37] The results of analysis are shown for the first BSC resonance at $\omega_c=0.3$ in Fig. 4(b). Indeed, roughly a half of branches of the BSC resonance shown by solid thick (blue) lines is stable while other branches shown by thin (red) lines are unstable. Thus, the BSC resonance is half stable.

As seen from Fig. 4 the more distance between the bound-state resonance and the linear one the less a width of the BSC resonance. Moreover, the first resonance is subjected to deformation compared to the next BSC resonances. Therefore one can expect further growth of E_{in} gives rise to coalescence of these resonances. In fact, the next Fig. 5 demonstrates this phenomenon that is especially complicated in real photonic crystal system as shown in Fig. 18.

Let us consider in which way an incident wave excites the bound state in the nonlinear FPR, i.e., an origin of the picket-fence type of resonances. By use of the complex eigenvalues of the effective Hamiltonian

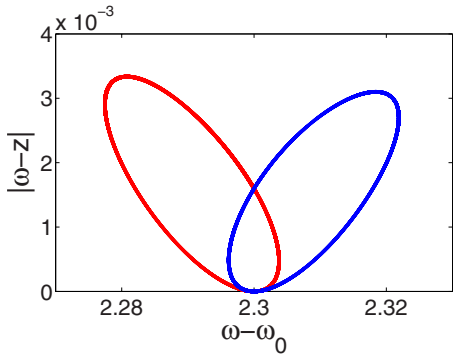

FIG. 6. (Color online) The frequency behavior of complex eigenvalues $|z_{1,2}-\omega|$ given by formula (23). $z=\omega_0+2.3$ defines the frequency of the BSC in the nonlinear FPR.

$$z_{1,2}=\frac{\omega_1+\omega_2}{2}-i\Gamma\pm\sqrt{\epsilon^2-\Gamma^2\exp(2i\theta)}, \tag{23}$$

which give positions [via Re(z)] and widths of the resonance states [via Im(z)] (Ref. 56) we obtain that at the point [Eq. (18)] one resonance becomes infinitely narrow [Im(z_1)=0] while the second one acquires the maximal width 2Γ.[31,35–38] Graphically the first resonance width behavior is demonstrated only in Fig. 6. Therefore the point [Eq. (18)] is the BSC, indeed.[30,58] At this point there is the homogeneous solution of LS [Eq. (16)] $|bound\rangle$ which is shared by the defect sites and by a piece of the one-dimensional waveguide between the defects with the amplitude $a_m=\sqrt{2\Gamma X_{cm}}$. In application to the real PhC waveguide coupled to the off-channel defects that conclusion is well illustrated below in Figs. 15(c), 17(c), and 17(d).

If the LS equation (16) were linear ($\lambda=0$) the necessary and sufficient condition for the existence of the inhomogeneous solution of this equation for $E_{in}\neq 0$ was that the left eigenvector $\langle bound|=(1-e^{i\theta_m})$ of the matrix $\omega-H_{eff}$ is to be orthogonal to the incoming vector $\binom{1}{e^{i\theta_m}}$ in the LS equation (16).[59] It holds indeed. Then the general solution of Eq. (16) at the BSC point for the linear case is given[27,28] by linear superposition

$$|\psi\rangle=\alpha\begin{pmatrix}1\\-e^{i\theta_m}\end{pmatrix}+E_{in}\sqrt{\Gamma/2}\begin{pmatrix}1\\e^{i\theta_m}\end{pmatrix}, \tag{24}$$

where α is an arbitrary coefficient and the second term is the particular solution of Eq. (16). The orthogonality of the BSC to incoming wave vector implies that the BSC is not coupled to the continuum and, therefore, there cannot be a resonance at its discrete energy $\omega_c=\omega_0$ for the linear transmission. That is *not the case* for the nonlinear system. A nonlinearity makes the linear superposition [Eq. (24)] invalid. As the result the interaction between the BSC and incoming wave appears because of nonlinearity. Therefore the incoming wave excites the BSC. Numerics indeed show that the positions of the picket-fence spectrum are at the BSC frequencies [Eq. (22)]. Moreover even for $e_{in}\to 0$ the coefficient α of the bound state in Eq. (24) is not arbitrary for the nonlinear case because the intensity of the bound state is quantized by Eq. (22).

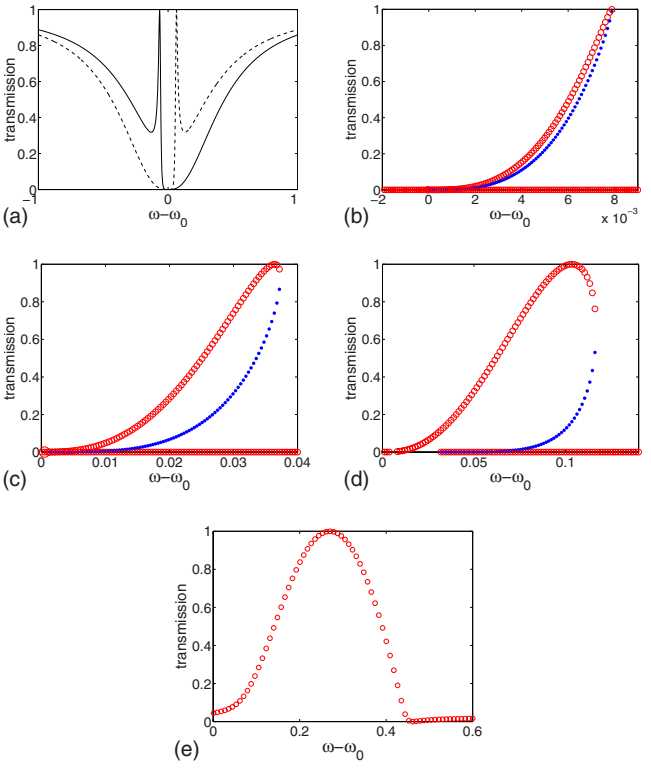

FIG. 7. (Color online) (a) Transmission spectra of the linear FPR for $\theta=\pi+0.1\pi$ (solid line) and $\theta=\pi-0.1\pi$ (dashed line). [(b)–(e)] The transmission given by Eq. (11) in the nonlinear FPR for the parameters $\Gamma=1$, $\theta_0=\pi$, and $\theta_1=\pi$. The incident power (b) $E_{in}=0.002$, (c) $E_{in}=0.01$, (d) $E_{in}=1$, and (e) $E_{in}=3$. Red open circles indicate a stable branch of the transmission while blue points do the unstable branch.

Furthermore let us consider the special case of the nonlinear FPR which already for linear case supports the BSC, i.e., $k(\omega_0)L=\pi m$ or $\theta_0=\pi m$. In the linear FPR for $\theta\to\pi m$ the width of the Fano resonance limits to zero (the collapse of the Fano resonance[27,34]) as shown in Fig. 7(a). From Eqs. (21) and (22) it follows that for the nonlinear case the BSC takes place at $\omega_c=\omega_0$, with an intensity at off-channel nonlinear defects equaled to zero: $X_c=0$. Therefore we obtain that the BSC has zero amplitude, i.e., it is to be empty. Only for the frequency deviated from ω_c the intensities X and Y arise at the defects as shown in Fig. 8. Correspondingly, for the low input amplitude E_{in} this frequency behavior will contribute into the frequency dependence of the transmission in accordance to formula (12) as shown in Fig. 7(b). However with further growth of the input amplitude the frequency behavior undergoes cardinal changes as shown in Figs. 7(c)–7(e). These anomalies in the transmission spectra reflect in the dependence of the outgoing power $P_{out}=TP$ on the incident one $P=\Gamma E_{in}^2$ (input-output characteristics). As different from usual input-output characteristics[1] the nonlinear FPR which supports BSC for zero input intensity the input-output characteristics displays extremely large efficiency for $\omega\to\omega_0$ as seen from Fig. 9. That results in extremely high efficiency in the input-output characteristics for small E_{in} as shown in Fig. 9. Thus a threshold for bistability over E_{in} tends to zero for $\omega\to\omega_0$ as different from the single nonlinear off-channel defect.[53]

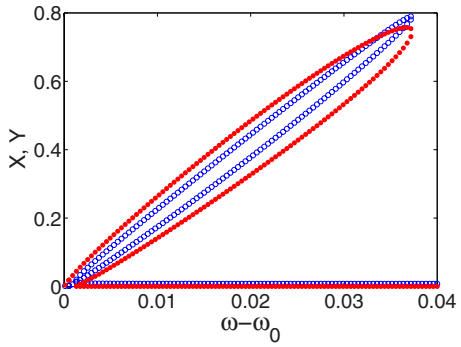

FIG. 8. (Color online) The solution of Eq. (15) for the nonlinear FPR model with parameters $\Gamma=1$, $\theta_0=\pi$, $\theta_1=\pi$, and $E_{in}=0.1$. X is shown by red points and Y is shown by blue open circles.

The results of stability analysis are shown in Figs. 7 and 9. One can see that the unstable branch in the transmission spectra is diminishing with growth of the input amplitude.

One may ask can the different nonlinear defects trap a wave? For the linear case it is impossible. Let the defects have frequencies $\omega_1=\omega_{01}+\lambda_1 X$ and $\omega_2=\omega_{02}+\lambda_2 Y$ and the coupling constants with the continuum Γ_1 and Γ_2, respectively. The coupled mode Eq. (11) is to be corrected as follows:

$$(\omega-\omega_1+i\Gamma_1)E_1+i\sqrt{\Gamma_1\Gamma_2}e^{i\theta}E_2=i\sqrt{\Gamma_1}E_{in},$$

$$i\sqrt{\Gamma_1\Gamma_2}e^{i\theta}E_1+(\omega-\omega_2+i\Gamma_2)E_2=i\sqrt{\Gamma_2}e^{i\theta}E_{in}. \quad (25)$$

In order both defects reflect perfectly at the same frequency we are to write

$$\omega_c=\omega_{01}+\lambda_1 X_c=\omega_{02}+\lambda_2 Y_c. \quad (26)$$

Here we took into account that the BSC can exist for zero input amplitude, i.e., it is the solution of the LS equation (25) for $E_{in}=0$. That condition gives us $\Gamma_1 E_1+\Gamma_2 E_2 e^{i\theta_n}=0$ or $Y_c=(\frac{\Gamma_1}{\Gamma_2})^2 X_c$. Then we obtain from Eq. (26)

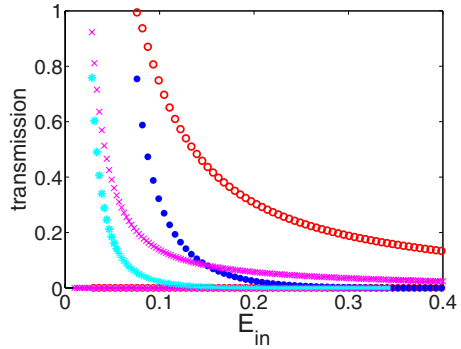

FIG. 9. (Color online) Input-output characteristics of the nonlinear FPR for the parameters given in Fig. 8. The case $\omega-\omega_0=0.03$ is shown by red open circles (stable solution) and by blue points (unstable solution). The case $\omega-\omega_0=0.015$ is shown by pink crosses (the stable solution) and by blue small stars (the unstable one).

$$X_c=\frac{\omega_{02}-\omega_{01}}{\lambda_1-\lambda_2\left(\frac{\Gamma_1}{\Gamma_2}\right)^2},\quad \omega_c=\frac{\lambda_1\omega_{02}-\lambda_2\omega_{01}\left(\frac{\Gamma_1}{\Gamma_2}\right)^2}{\lambda_1-\lambda_2\left(\frac{\Gamma_1}{\Gamma_2}\right)^2},\quad X_c>0. \quad (27)$$

Finally substituting Eq. (27) into Eq. (6) we obtain that different nonlinear defects may trap wave indeed, if the distance between defects is discrete as in the linear case while for the FPR with identical nonlinear defects the condition for the distance is free.

III. TIGHT-BINDING MODEL OF THE NONLINEAR FABRY-PEROT SYSTEM

The theoretical approach based on a difference equation formulation for fields in the two-dimensional waveguide channels and off-channel nonlinear impurities coupled to the waveguide was developed in papers by McGurn.[6,47,48] The simplest model is a discrete tight-binding model that describes a linear chain coupled to a single-site off-channel defect with the instantaneous Kerr nonlinearity.[6,7] The model attracted interest long time ago because of analytical treatment and its generality.[2,6,7,9] The main result is that the transmission coefficient of a single waveguide mode scattering from Kerr off-channel features was shown to exhibit bistability properties arising from a nonlinearity of the off-channel site. In Refs. 12, 48, and 49 it was considered also an off-channel cavity comprised of two neighboring sites having different Kerr dielectric properties with similar effects as the off-channel cavity of the single-site defect. In the present section we consider the tight-binding model version of FPR with nonlinear mirrors, i.e., consists of the linear chain coupled with two nonlinear off-channel defects separated by N chain sites as shown in Fig. 1(c). In the linear case the model supports N BSCs with the eigenfrequencies $\omega_c=-2\cos(\frac{\pi n}{N+1})$, $n=1,2,\ldots,N$ if (i) the off-channel sites are identical and (ii) there is a perfect reflection from each off-channel defect at the frequency ω_c, which coincides with the resonant frequency of the off-channel defect.[40,41] Therefore the condition for BSCs in the linear FPR needs tuning of the defect resonance frequency to be equaled to the BSC frequency ($\omega_c=\omega_0$) that is rather subtle. We show that for the case of the nonlinear off-channel defects the condition becomes sufficiently soft.

We start with the simplest tight-binding linear chain coupled with two different nonlinear off-channel defects at the sites $n=0$ and $n=N+1$, respectively. Following Ref. 7 we write the Hamiltonian of the tight-binding model for the case in Fig. 1(d) as follows:

$$H=-\sum_n \psi_n\psi_{n+1}^*-u\psi_0\phi_1^*-u\psi_{N+1}\phi_2^*+\text{H.c.}+\omega_0|\phi_1|^2$$
$$+\frac{1}{2}\lambda|\phi_1|^4+\omega_0|\phi_2|^2+\frac{1}{2}\lambda|\phi_2|^4. \quad (28)$$

For the chain we write the solution as $\psi_n=\phi_{in}e^{ikn}+re^{-ikn}$, if $n\leq 0$, and $\psi_n=te^{ikn}$, if $n\geq N+1$. Here ϕ_{in} is the amplitude of

incident wave, $|r|^2/\phi_{in}^2$ and $|t|^2/\phi_{in}^2$ are the reflection and transmission probabilities, respectively. Let us, first, consider the simple case of the nearest off-channel defects, i.e., $N=0$. Then from the lattice Hamiltonian (28), we derive a system of coupled nonlinear dynamic equations[7]

$$\omega\psi_0 = -\psi_{-1} - \psi_1 + u\phi_1,$$

$$\omega\psi_1 = -\psi_{-}\psi_2 + u\phi_2,$$

$$\omega\phi_1 = \omega_1\phi_1 + u\psi_0,$$

$$\omega\phi_2 = \omega_2\phi_2 + u\psi_1,$$

where $\omega=-e^{ik}-e^{-ik}$ and $\omega_a=\omega_0+\lambda|\phi_a|^2$, $a=1,2$. After simple algebraic manipulations we can rewrite this system of equations as follows:

$$(\omega-\omega_1+i\Gamma_k)\phi_1 + i\Gamma_k\phi_2 e^{ik} = u\phi_{in},$$

$$i\Gamma_k\phi_1 e^{ik} + (\omega-\omega_1+i\Gamma_k)\phi_2 = u\phi_{in}e^{ik}, \tag{29}$$

$$t = \phi_{in}e^{ik} - i\Gamma_k\phi_1 e^{ik}/u - i\Gamma_k\phi_2/u, \tag{30}$$

where $\Gamma_k=\frac{u^2}{2\sin k}$ plays role of the width Γ in the Fan and Wang model (11). If the off-channel defects were separated by N sites we would substitute e^{ik} here by $e^{i(N+1)k}$. Comparison of Eqs. (29) and (30) with Eqs. (11) and (12) shows that the tight-binding model of the FPR gives the coupled mode Eq. (11) with accuracy of notations: $\Gamma_k=\Gamma$ and $\theta=k(N+1)$.

Resuming calculations performed in Sec. II [see Eqs. (13) and (15)] we obtain the self-consistency equations for $X=|\phi_1|^2$ and $Y=|\phi_2|^2$,

$$X[(\omega-\omega_0-\lambda X)^2(\omega-\omega_0-\lambda Y)^2 + \Gamma_k^2(2\omega-\omega_0-\omega_2-\lambda X-\lambda Y)^2] = u^2\phi_{in}^2(\omega-\omega_0-\lambda Y)^2,$$

$$Y[(\omega-\omega_0-\lambda X)^2(\omega-\omega_0-\lambda Y)^2 + \Gamma_k^2(2\omega-\omega_0-\omega_0-\lambda X-\lambda Y)^2] = u^2\phi_{in}^2(\omega-\omega_0-\lambda X)^2. \tag{31}$$

The total transmission probability calculated numerically for the tight-binding model of the FPR with four sites ($N=4$) between two off-channel nonlinear defects is shown in Fig. 10 which is similar to the results shown in Fig. 3(a). Although the linear model can have four BSCs $\omega_c=-2\cos(\pi n/5)$, $n=1,2,3,4$, the nonlinear model has the BSCs if $\omega_c=\omega_1=\omega_0+\lambda X_c$. Therefore there are BSCs only for $\omega>\omega_0$ if $\lambda>0$. For $\omega_0=-1.5$ as given in Fig. 10 we obtain that there are three bound states for three quantized values of the field intensity X_c. Correspondingly, one can see three BSC resonances in Fig. 10. The frequency behavior of the intensities at the defects has the form similar to Fig. 3. Thus, the only difference between continual and discrete models is restricted band of the wave propagation and restricted number of the BSC resonances.

IV. CALCULATIONS IN PHOTONIC CRYSTAL

The coupling-mode theory models the Fabry-Perot interferometer (the Fan *et al.* model[36,37]) described in Sec. II has

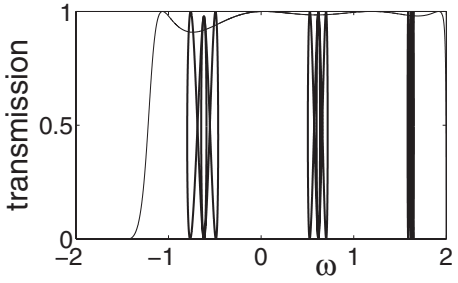

FIG. 10. Transmission spectra as dependent on frequency in the tight-binding model of FPR shown in Fig. 1(c) for the case of four ($N=4$) sites between nonlinear mirrors. The parameters of the FPR presented in Hamiltonian (28) are $u=0.5$, $\omega_0=-1.5$, $\lambda=0.008$, and $\phi_{in}=0.1$.

remarkable advantages. First, it allows us to treat the transmission through the linear FPR analytically. Second, the model presents exclusively transparent and clear arguments for the frequencies and amplitudes of the BSCs even in the nonlinear FPR [see formula (22)]. The price for simplicity of the model is free parameters which are to be calculated for consideration of real photonic crystal structures and limitations related to the effects of the waveguide dispersion at the band edges.[10] These limitations can be easily avoided by an use of the tight-binding model described in Sec. III. However even this model is very far of reality because of that the approximation of the nearest-neighbor interaction is very crude in many cases.[60] As a result computation of transmission in the real PhC is rather complicated task even in the linear case but becomes formidable for the nonlinear case.

As shown in Ref. 61, the Green's function approach allows one to obtain very accurate results for rather complex geometries of the photonic circuits compared to more time-consuming direct numerical finite-difference time-domain simulations. Moreover, this approach allows to include into PhC the defect rods of the Kerr medium and reduce the Maxwell equations to discrete nonlinear equations[60] provided that the radius of the defect rods is sufficiently small so that the electric field is almost constant inside the defect rods. Far from the defects in waveguide the EM field is seeking in the form of incident and reflected or transmitted waves[10,62] that allows to obtain the self-consistency equations for the field at the nonlinear defects.

A different approach is based on an expansion of the electromagnetic field over the maximally localized photonic Wannier functions that leads to effective lattice models of the PhC structures.[46] Taking the solution as incident, reflected far left from the scattering region and transmitted far right from it the solution inside the scattering region can be written in the Lippman-Schwinger equation form

$$(H_{eff}-\omega)|\Psi_S\rangle = E_{in}\hat{V}|inc\rangle. \tag{32}$$

Details of derivation of this equation are given in Ref. 23. Equation (32) is similar to Eq. (16) which is exactly the coupled mode Eq. (11) however in the case of real PhC the state $|\Psi_S\rangle$ includes around hundred of cells inside the scattering region.[23] Respectively, the rank of the effective Hamil-

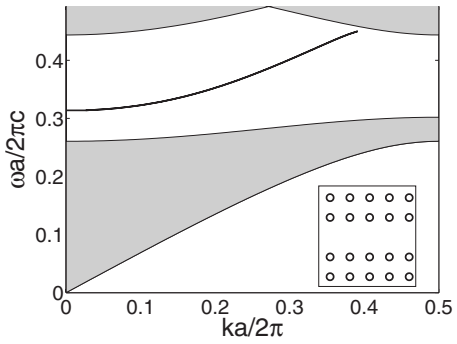

FIG. 11. The dispersion relation of the propagating guided TM mode (Ref. 46) in the PhC described in the text.

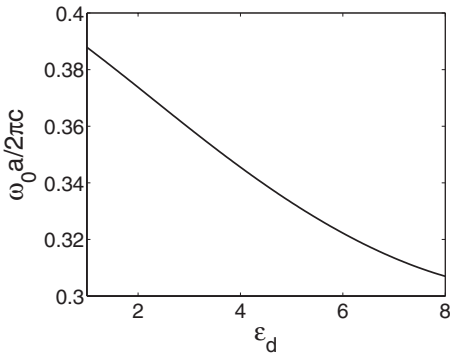

FIG. 12. The frequency of isolated bound mode for the single isolated defect cylinder as dependent on its dielectric constant ϵ_d (Refs. 23 and 46).

tonian in Eq. (32) reaches also the same amount. The waves in the waveguide spread over decade of cells cross to waveguide far from the scattering region. This approach allows us to search the bound states from the equation $H_{eff}|bound\rangle = \omega_c|bound\rangle$. If some of rods are made from a Kerr medium, then the solution $|\Psi_S\rangle$ is to be subjected to the procedure of self-consistency at the Kerr medium cells. Numerically, we solved algebraic equations for each of hundred cells centered at rods belong to the scattering region, including two nonlinear algebraic self-consistent equations at the nonlinear rods.

The PhC Fabry-Perot structures formed by two linear cavities in the photonic waveguide (in-channel defects) and near by (off-channel defects) were considered in Refs. 22 and 23, respectively. We consider the square lattice (lattice constant a) of cylindrical dielectric rods of radius $0.18a$ and dielectric constant $\epsilon=11.56$ (GaAs at the wavelength 1.5 μm) in air as given in Refs. 38 and 46. Removing a row of rods creates the single-mode PhC waveguide with effective width of order of a few a.[1,38,46] The waveguide supports a single wide band of guided mode spanning from 0.302 to the upper band edge 0.444 (Ref. 46) as shown in Fig. 11 for reader's convenience.

All quantities in numerics are dimensionless, the frequency $\tilde{\omega}=\omega a/2\pi c$, electric field E, and the constant of nonlinearity λ. Let us evaluate these constants for real PhC waveguide with defect rods. The optical Kerr effect introduced by formula (3) is described by the nonlinear refractive index n_2 for linearly polarized light[50,63] $n=n_0+n_2I$, where n_0 is the linear refractive index and I is an intensity of light. We take in numerical calculations the incident power per length of order 100 mW/a. Then the incident intensity equals $I_0=100$ mW/a^2. For chosen period of the PhC lattice $a=0.5$ μm we obtain that the incident intensity equals 0.04 GW/cm^2. A change in the frequency at the defect similar to Eq. (4) can be written as

$$\tilde{\omega}(n) = \tilde{\omega}(n_0) + \tilde{\omega}' n_2 I_d = \tilde{\omega}_0 + \tilde{\omega}' n_2 I_0 |E|^2, \tag{33}$$

where $|E|^2=I_d/I_0$ is the dimensionless intensity at the defects. Then it follows from that

$$\lambda = \tilde{\omega}' n_2 I_0. \tag{34}$$

In the first series of computations we take the linear and nonlinear refractive indexes of the defect rods are, respectively, $n_0=\sqrt{\epsilon_0}=\sqrt{5}$ and $n_2=2\times10^{-12}$ cm^2/W. The corresponding unperturbed linear eigenmode of the isolated defect has the frequency $\tilde{\omega}_0=0.333$. From graphics for the dependence $\tilde{\omega}_0$ on the dielectric constant $\epsilon_d=n^2$ (Fig. 12) and Fig. 11 we find that the dimensionless light velocity $\tilde{\omega}'$ is around -10^{-2}. Finally substituting all these estimates into Eq. (34) we obtain $\lambda\sim-10^{-5}$ which is much less than we used in the model cases. We start here with presentation in Fig. 13 the amplitudes $|E_1|$ and $|E_2|$ at the defects computed self-consistently as dependent on the frequency $\tilde{\omega}$. If to compare Fig. 13(b) to corresponding Fig. 3(b) one can find good qualitative agreement between the Fan *et al.*[36] model and real PhC structure except that long loops around the BSC point are decreasing with growth of the frequency. That is related to the sign of the nonlinearity constant λ in formula (4). The bottom part of the frequency behavior of $|E_1|$ and $|E_2|$ in Fig. 13(a) is related to usual resonant enhancement of the intensities at the eigenfrequency of the defects $\tilde{\omega}_0=0.333$ as one can see from Fig. 14. However the another branch of the solution shown in Fig. 13(b) is related to the BSC similar to the model results shown in Fig. 3. This branch changes with growth of the incident power as shown in Fig. 3(b). Although as one can see from Fig. 3(c) a growth of input amplitude two times leads to the same amount of increasing for $|X-X_c|$ and $|Y-Y_c|$, the relative change in the intensities at the defects $\frac{|X-X_c|}{X_c}$ and $\frac{|Y-Y_c|}{Y_c}$ is rather small. That observation is close to that the BSC has low response to the incident power as shown below in Figs. 17(c) and 17(d).

In the forthcoming figures we show the solutions of the LS equation (32) for different frequencies and different branches of the solution. Figure 15(a) shows the absolute value of EM field for the resonant case marked by star in Fig. 14, i.e., for the frequency $\tilde{\omega}=\tilde{\omega}_0=0.333$. Similar to the linear case we see resonant enhancement of the field at the defects complimented by low wave flow in the waveguide. Next, we consider $\tilde{\omega}=\tilde{\omega}_c=0.3279$, where $\tilde{\omega}_c$ is the frequency of the BSC marked by open circle in Fig. 14. In general there are five solutions (branches) at the vicinity of the BSC frequency $\tilde{\omega}_c$. However at this frequency two pairs of the branches are crossed. They are marked by cross and diamond. The last branch is inherited from the linear case and marked by filled circle. The corresponding wave function for small λ is close to nonresonant linear transmission and shown in Fig. 15(b).

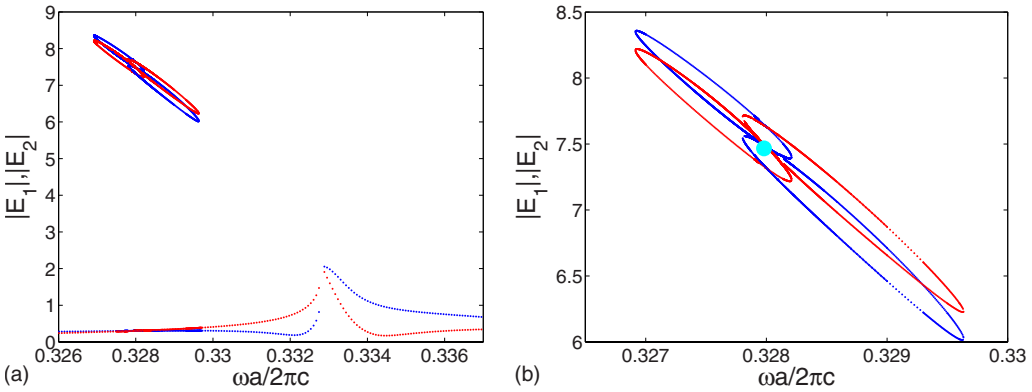

FIG. 13. (Color online) (a) Whole self-consistent solution for the EM field at the nonlinear defects in the PhC structure shown in Fig. 1(a). (b) Blow up of the solution near the BSC point shown by blue point. The amplitude at the first nonlinear defect rod $|E_1|$ is shown by red and the amplitude at the second defect rod $|E_2|$ is shown by blue. The parameters of the PhC are the following $a=0.5$ μm, $r_d=0.18a$, $\epsilon=11.56$, $\epsilon_0=5$, $\omega_0=0.333$, and $n_2=2\times10^{-12}$ cm^2/W the input power per length 100 mW/a.

Other two solutions marked by cross and diamond are exclusively result of nonlinearity. For $E_{in}\to 0$ both solutions limit to the BSC point. Respectively, the solution of Eq. (32) goes to the BSC wave function. However even for the finite but small input power the wave functions obtained for the solutions marked by star and diamond in Fig. 14 are very close to BSC because of smallness λ as Fig. 15(c) shows. One can see that this state is localized near by the defects and in the waveguide between the defects if full correspondence to the conclusion obtained in the Wang and Fan model. The wave function corresponded to the case marked by diamond in Fig. 14 is also very close to the BSC. For the frequency of the BSC $\tilde{\omega}_c=0.3279$ one can find from Fig. 11 corresponding wave number $Lk_c/\pi\approx 0.9927$. Then the value $4k_ca$ is very close to π, i.e., the BSC which obeys to Eq. (19) is classified by $m=1$ and, therefore, is to be even relative to up and down. Respectively, the particular transport solution presented in Eq. (24) at right hand is too odd. Figures 16(a) and 16(b) which shows phase of the wave function remarkably confirm this simple model conclusions for consideration of real PhC structure.

Both cases shown in Figs. 15(a) and 15(b) inherit from the linear FPR and, therefore, have intensity proportional to the incident one E_{in}^2. That is demonstrated in Figs. 17(a) and 17(b). It is not the case for the new branch of the transmission marked by cross in Fig. 14. That point is result of excitement of the BSC by incident wave via nonlinearity of defects. Therefore one can expect that the intensity of the BSC will slightly change if we substantially change the incident intensity, say, four times because of smallness of λ. Figures 17(c) and 17(d) demonstrate that conclusion, indeed.

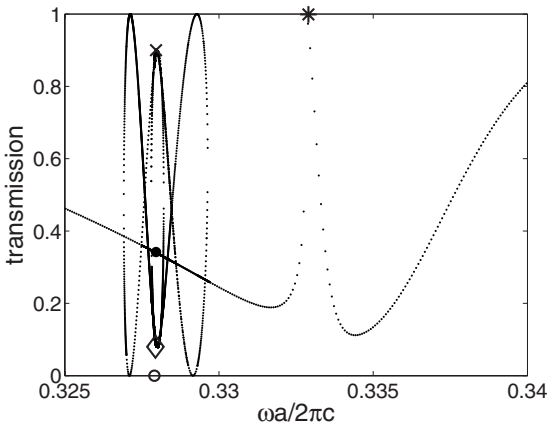

FIG. 14. Transmission spectra in the PhC structure for the same parameters given in previous figure. The BSC frequency $\tilde{\omega}_c=0.3279$ is marked by open circle.

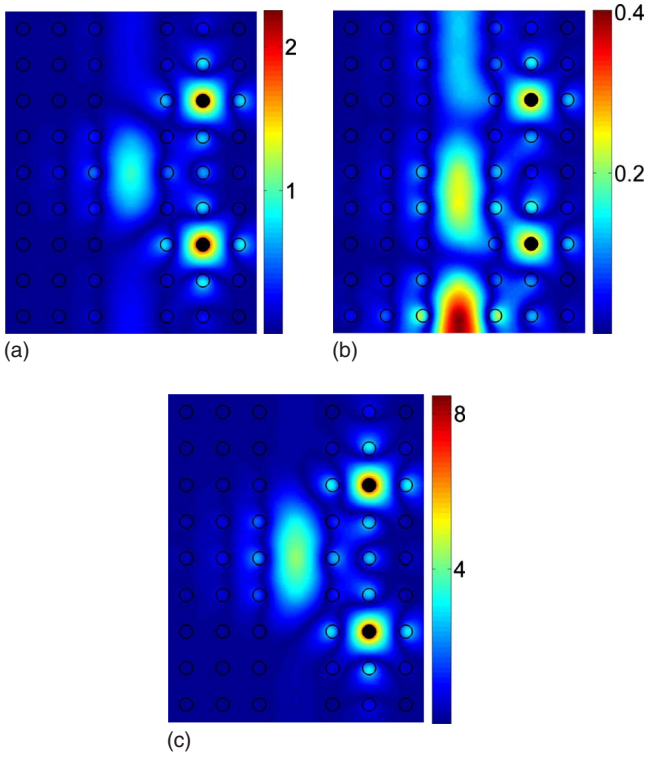

FIG. 15. (Color online) The absolute values of EM field for (a) the resonant case for $\tilde{\omega}=\tilde{\omega}_0=0.333$ marked in Fig. 14 by star, (b) for the BSC frequency $\tilde{\omega}=\tilde{\omega}_c=03279$ marked by filled circle in Fig. 14, and (c) for the same frequency $\tilde{\omega}_c=03279$ however for the different branch marked by cross in Fig. 14. The wave function shown in (c) tends to the BSC for $E_{in}\to 0$. The incident power per length is chosen 100 mW/a.

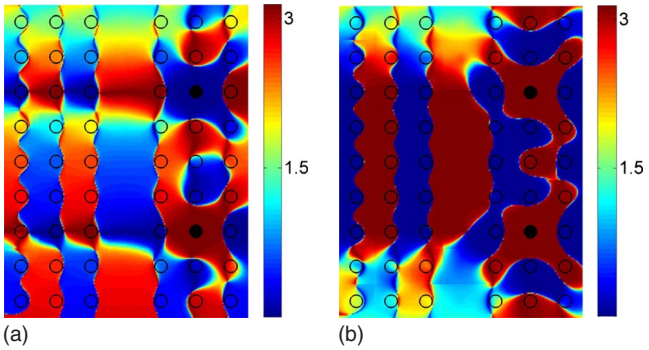

FIG. 16. (Color online) Phase structure of (a) the transport solution shown in Figs. 15(b) and 15(b) the solution shown in Fig. 15(c) which is close to the BSC.

As seen from Fig. 13 a smallness of the nonlinearity constant λ needs very large intensity at the defect rods to obtain the BSC. However there are the Kerr-media materials which have the nonlinear coefficient λ close to that used in models. For example, n_2 is of order 10^{-10} cm^2/W in an Al_2O_3 matrix doped with Cu nanoparticles $n_2=2.9\times10^{-10}$ cm^2/W,[64] in silicate glasses doped with Ag nanoparticles $n_2=-6.2\times10^{-10}$ cm^2/W,[65] in doped poly(β pinene) $n_2=1.45\times10^{-10}$ cm^2/W.[66]

In the second series of numerical calculation we have chosen $n_2=3.5\times10^{-10}$ cm^2/W. This amount of the nonlinear refractive index corresponds to $\lambda\sim10^{-3}$ for the input intensity per length 100 mW/a, i.e., roughly 100 times exceeds the former case. The BSC frequencies might be only less than the defect eigenfrequency ω_0 because of $\lambda<0$. As

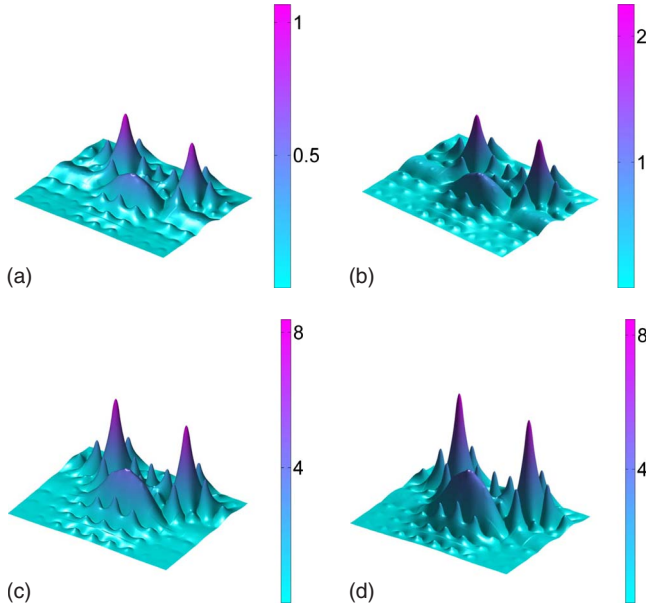

FIG. 17. (Color online) [(a) and (b)] The three-dimensional plot of the absolute value of the transport solution for the resonant case $\tilde{\omega}=0.333$ as in Fig. 15(a) however for the two values of the incident power (a) 25 mW/a and (b) 100 mW/a. The cases (c) and (d) show the absolute value of the solution closed to the BSC shown in Fig. 15(c) for two amounts of the incident power (c) 25 mW/a and (d) 100 mW/a.

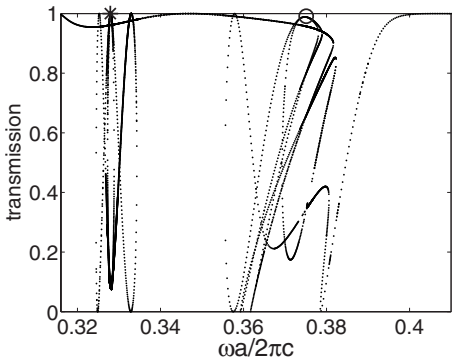

FIG. 18. Transmission spectra in the PhC structure with the same parameters as in Fig. 14 but for different the nonlinear defects with the parameters $\epsilon_0=1.1$, $\omega_0=0.3865$, and $n_2=3.5\times10^{-10}$ cm^2/W. The incident power per length is 100 mW/a. The first BSC frequency $\tilde{\omega}_c=0.3279$ is marked by star and the second one is marked by open circle $\tilde{\omega}_c=0.3751$.

Fig. 14 shows there is the only bound state below $\omega_0=0.333$ with the frequency $\tilde{\omega}_c=0.3279$ for the first series of calculations with the defect dielectric constant $\epsilon_0=5$. For the second choice we take the defect dielectric constant $\epsilon_0=1.1$ which gives the eigenfrequency of the isolated defect $\omega_0=0.3865$. Respectively, we obtain two BSCs between 0.3865 and the bottom of the propagation band 0.302. All other structure parameters are the same as was used in the first series. The transmission spectra for that choice plotted in Fig. 18 shows two BSC resonances with the first BSC frequency $\tilde{\omega}_{c1}=0.3279$ and the second one $\tilde{\omega}_{c2}=0.3751$. The second resonance is strongly mixed with the linear FPR one. As it may be calculated from Fig. 11 the corresponding wave numbers correspond to $Lk_{c1}/\pi\approx0.9993$ and $Lk_c/\pi\approx1.9992$, i.e., $m=1$ and 2. That result nicely agrees with phase pictures of the BSCs in Fig. 19. Finally we show here only phase of the BSCs in Fig. 19 in order to demonstrate the simple phase rule [Eq. (19)]. The first state in Fig. 19(a) corresponds to even one while the second state in Fig. 19(b) does to the odd one. One can see that the phase of BSCs is mostly 0 or π, i.e., the BSCs are real functions.

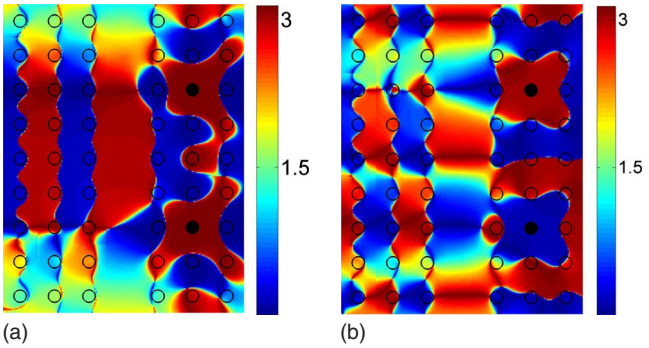

FIG. 19. (Color online) Phase structures of the states close to the (a) first even BSCs with the frequency $\tilde{\omega}_{c1}=0.3279$ and (b) the second odd one with the frequency $\tilde{\omega}_{c2}=0.3751$. The states are marked in Fig. 18 by star and open circle, respectively.

V. CONCLUSIONS

In the FPR the nonlinear off-channel defects self induce the transmission zeroes at whole discrete sequence of the light intensity to give rise to a corresponding sequence of bound states. These solutions exist for $E_{in}=0$ that determines them as the BSCs in continuum. On the other hand, nonlinearity of the off-channel defects provides a coupling of incident wave with the BSCs to cause new resonances at their eigenfrequencies. Moreover, as seen in Figs. 4 and 5 the FPR might be transparent in the vicinity of these resonances. These results were obtained in two series of numerical calculations in real photonic crystal structures with two defects made of a Kerr media and well agreed with the results of model theories, the coupled-mode theory in Sec. II and the tight-binding model in Sec. III. The self-induced BSC resonances as shown in Figs. 4, 10, and 14 have the shape of butterfly in all approaches if they are far from the usual resonance inherited from the linear system. However not all branches in this butterfly shape resonance is stable as shown in Fig. 4(b). However the stable part of the BSC resonance is quite enough to observe it.

Nonlinearity reveals important conceptual aspects of the bound states which in general were discussed already in Ref. 32. We mention two of them in application to the Fabry-Perot interferometer with nonlinear "mirrors," fabricated from the Kerr-media off-channel defects. If the defect were linear there would be only the eigenfrequency ω_0 of the defect at which the mirror is perfect. Therefore the condition for the BSC takes the form $k(\omega_0)L=\pi m$, i.e., can be fulfilled for discrete values of the distance between linear defects that is hardly achievable in the discrete PhC waveguide. Or one can tune the dielectric constant of the defects.[36] The nonlinear defects perfectly reflect at the frequency $\omega_0+\lambda|E_a|^2$, $a=1,2$. Respectively, there is new possibility to satisfy the boundary condition for the BSC by a quantization of the intensity of electromagnetic wave $|E_a|^2$ at the defects as written in Eq. (22) irrespective to the distance between the nonlinear mirrors and their eigenfrequency ω_0. That constitutes the first important aspect of the BSCs in the nonlinear FPR.

The second important aspect of the nonlinear FPR which was not considered yet is that these BSCs become visible for wave which incidents and goes through. Mathematically it is related with that the linear superposition of transport solution and the BSC [Eq. (24)] cannot be anymore by the solution of basic equations (the coupled-mode equations for the EM transmission, or the LS equation for the quantum case) for the nonlinear case. As a result incident wave couples with the BSC to give rise to a very peculiar shape of resonances shown in Figs. 3, 7, 10, 14, and 18. For small incident amplitude E_{in} the positions of the BSC induced resonances are just at the frequencies of BSCs. However with growth of the incident power the width of the BSC induced resonances is increased to give rise to a coalescence of "new" resonances with "old" ones which take place in the linear case. Obviously, that opens much room in manipulation by bistability properties of the BSCs which were shown Figs. 7 and 9.

ACKNOWLEDGMENTS

The work was partially supported by RFBR under Grant No. 09-02-98005 "Siberia." We are greatly acknowledge Konstantin Pichugin for many discussions.

[1] J. Joannopoulos, S. G. Johnson, J. N. Winn, and R. D. Meade, *Photonic Crystals: Molding the Flow of Light* (Princeton University Press, Princeton, NJ, 2008).
[2] M. I. Molina and G. P. Tsironis, Phys. Rev. B **47**, 15330 (1993).
[3] B. C. Gupta and K. Kundu, Phys. Rev. B **55**, 894 (1997); **55**, 11033 (1997).
[4] M. I. Molina, Phys. Rev. B **67**, 054202 (2003).
[5] A. R. Cowan and J. F. Young, Phys. Rev. E **68**, 046606 (2003).
[6] A. R. McGurn, Chaos **13**, 754 (2003); J. Phys.: Condens. Matter **16**, S5243 (2004).
[7] A. E. Miroshnichenko, S. F. Mingaleev, S. Flach, and Yu. S. Kivshar, Phys. Rev. E **71**, 036626 (2005).
[8] A. E. Miroshnichenko and Yu. S. Kivshar, Phys. Rev. E **72**, 056611 (2005).
[9] S. Longhi, Phys. Rev. B **75**, 184306 (2007).
[10] S. F. Mingaleev, A. E. Miroshnichenko, Yu. S. Kivshar, and K. Busch, Phys. Rev. E **74**, 046603 (2006).
[11] A. E. Miroshnichenko, Yu. Kivshar, C. Etrich, T. Pertsch, R. Iliew, and F. Lederer, Phys. Rev. A **79**, 013809 (2009).
[12] A. E. Miroshnichenko, Phys. Rev. E **79**, 026611 (2009).
[13] J. H. Marburger and F. S. Felber, Phys. Rev. A **17**, 335 (1978).
[14] W. Chen and D. L. Mills, Phys. Rev. B **35**, 524 (1987); **36**, 6269 (1987).
[15] R. Reinisch, G. Vitrant, and M. Haelterman, Phys. Rev. B **44**, 7870 (1991).
[16] J. von Neumann and E. Wigner, Phys. Z. **30**, 465 (1929).
[17] F. H. Stillinger and D. R. Herrick, Phys. Rev. A **11**, 446 (1975).
[18] D. R. Herrik, Physica **85B**, 44 (1977).
[19] F. H. Stillinger, Physica **85B**, 270 (1977).
[20] F. Capasso, C. Sirtori, J. Faist, D. L. Sivco, S.-N. G. Chu, and A. Y. Cho, Nature (London) **358**, 565 (1992).
[21] A. F. Sadreev, E. N. Bulgakov, K. N. Pichugin, I. Rotter, and T. V. Babushkina, in *Quantum Dots, Research, Technology and Applications*, edited by R. W. Knoss (Nova Sciences, Hauppauge, NY, 2008), pp. 547–577.
[22] C. Manolatou, M. J. Khan, S. Fan, P. R. Villeneuve, H. A. Haus, and J. D. Joannopoulos, IEEE J. Quantum Electron. **35**, 1322 (1999).
[23] E. N. Bulgakov and A. F. Sadreev, Phys. Rev. B **78**, 075105 (2008).
[24] D. C. Marinica, A. G. Borisov, and S. V. Shabanov, Phys. Rev. Lett. **100**, 183902 (2008).
[25] A. E. Miroshnichenko, S. Flach, and Y. S. Kivshar, arXiv:0902.3014 (unpublished).
[26] N. Prodanović, V. Milanović, and J. Radovanović, J. Phys. A **42**, 415304 (2009).
[27] A. F. Sadreev, E. N. Bulgakov, and I. Rotter, Phys. Rev. B **73**, 235342 (2006).

[28] A. F. Sadreev, E. N. Bulgakov, and I. Rotter, JETP Lett. **82**, 498 (2005).
[29] A. Z. Devdariani, V. N. Ostrovsky, and Yu. N. Sebyakin, Sov. Phys. JETP **44**, 477 (1976).
[30] H. Friedrich and D. Wintgen, Phys. Rev. A **32**, 3231 (1985).
[31] A. Volya and V. Zelevinsky, Phys. Rev. C **67**, 054322 (2003).
[32] E. N. Bulgakov and A. F. Sadreev, Phys. Rev. B **80**, 115308 (2009).
[33] H. A. Haus, *Waves and Fields in Optoelectronics* (Prentice-Hall, New York, 1984).
[34] C. S. Kim, A. M. Satanin, Y. S. Joe, and R. M. Cosby, Phys. Rev. B **60**, 10962 (1999).
[35] S. Fan, P. R. Villeneuve, J. D. Joannopoulos, and H. A. Haus, Phys. Rev. Lett. **80**, 960 (1998).
[36] S. Fan, P. R. Villeneuve, J. D. Joannopoulos, M. J. Khan, C. Manolatou, and H. A. Haus, Phys. Rev. B **59**, 15882 (1999).
[37] Z. Wang and S. Fan, Phys. Rev. E **68**, 066616 (2003).
[38] L.-L. Lin, Z.-Y. Li, and B. Lin, Phys. Rev. B **72**, 165330 (2005).
[39] C. S. Kim and A. M. Satanin, Phys. Rev. B **58**, 15389 (1998).
[40] I. Rotter and A. F. Sadreev, Phys. Rev. E **69**, 066201 (2004); **71**, 046204 (2005).
[41] A. F. Sadreev, E. N. Bulgakov, and I. Rotter, J. Phys. A **38**, 10647 (2005).
[42] G. Ordonez, K. Na, and S. Kim, Phys. Rev. A **73**, 022113 (2006).
[43] Y. Xu, Y. Li, R. K. Lee, and A. Yariv, Phys. Rev. E **62**, 7389 (2000).
[44] S. Hughes, Phys. Rev. Lett. **98**, 083603 (2007).
[45] P. R. Villeneuve, S. Fan, and J. D. Joannopoulos, Phys. Rev. B **54**, 7837 (1996).
[46] K. Busch, S. F. Mingaleev, A. Garcia-Martin, M. Schillinger, and D. Hermann, J. Phys.: Condens. Matter **15**, R1233 (2003).
[47] A. R. McGurn and G. Birkok, Phys. Rev. B **69**, 235105 (2004).
[48] A. R. McGurn, Adv. OptoElectron. **2007**, 92901.; Phys. Rev. B **77**, 115105 (2008).
[49] S. F. Mingaleev, A. E. Miroshnichenko, and Y. S. Kivshar, Opt. Express **15**, 12380 (2007); **16**, 11647 (2008).
[50] D. C. Hutchings and B. S. Wherrett, Phys. Rev. B **50**, 4622 (1994).
[51] J. Bravo-Abad, A. Rodriguez, P. Bermel, S. G. Johnson, J. D. Joannopoulos, and M. Soljačić, Opt. Express **15**, 16161 (2007).
[52] S. Fan, W. Suh, and J. D. Joannopoulos, J. Opt. Soc. Am. A Opt. Image Sci. Vis. **20**, 569 (2003).
[53] M. F. Yanik, S. Fan, and M. Soljačić, Appl. Phys. Lett. **83**, 2739 (2003).
[54] A. F. Sadreev and I. Rotter, J. Phys. A **36**, 11413 (2003).
[55] H. Feshbach, Ann. Phys. (N.Y.) **5**, 357 (1958); **19**, 287 (1962).
[56] I. Rotter, Rep. Prog. Phys. **54**, 635 (1991).
[57] V. V. Sokolov and V. G. Zelevinsky, Ann. Phys. **216**, 323 (1992).
[58] E. N. Bulgakov, I. Rotter, and A. F. Sadreev, Phys. Rev. A **75**, 067401 (2007).
[59] V. I. Smirnov, *A Course of Higher Mathematics* (Pergamon, Oxford, 1964), Vol. 3.
[60] S. F. Mingaleev, Yu. S. Kivshar, and R. A. Sammut, Phys. Rev. E **62**, 5777 (2000).
[61] S. F. Mingaleev and Yu. S. Kivshar, Opt. Lett. **27**, 231 (2002).
[62] N. Marzari and D. Vanderbilt, Phys. Rev. B **56**, 12847 (1997).
[63] R. E. de Araujo and A. S. L. Gomes, Phys. Rev. A **57**, 2037 (1998).
[64] J. M. Ballesteros, R. Serna, J. Solis, C. N. Afonso, A. K. Petford-Long, D. H. Osborne, and R. F. Haglund, Jr., Appl. Phys. Lett. **71**, 2445 (1997).
[65] R. A. Ganeev, A. I. Ryasnyansky, A. L. Stepanov, and T. Usmanov, Opt. Quantum Electron. **36**, 949 (2004).
[66] H. Rajagopalan, P. Vippa, and M. Thakura, Appl. Phys. Lett. **88**, 033109 (2006).